EFB Bioeconomy Journal 2 (2022) 100024

Contents lists available at ScienceDirect

EFB Bioeconomy Journal

journal homepage: www.elsevier.com/locate/bioeco

Influence of ultrasound and cation substitution on the intercalation of organic anions to the Mg_3/Al_1 layered double hydroxide

Ligita Valeikiene*, Kamile Kriukaite, Inga Grigoraviciute-Puroniene, Anton Popov, Aivaras Kareiva

Institute of Chemistry, Vilnius University, Naugarduko 24, LT 03225, Vilnius, Lithuania

ARTICLE INFO

Keywords:
Layered double hydroxides
Sol-gel method
Ultrasound
Transition metals
Intercalation, Anion exchange

ABSTRACT

The Mg_3/Al_1 and $Mg_{3-x}M_x/Al_1$ (M = Mn, Co, Ni, Cu, Zn) layered double hydroxides (LDHs) were synthesized using sol-gel synthesis technique. The intercalation with different organic anions (formate ($HCOO^-$), acetate (CH_3COO^-), oxalate ($C_2O_4^{2-}$), tartrate ($C_4H_6O_4^{2-}$) and citrate ($C_6H_5O_7^{3-}$)) using ion exchange approach was investigated. The influence of ultrasound and cation substitution on the intercalation of organic anions to the Mg_3/Al_1 LDH has been investigated. The obtained results indicated that ultrasound has a positive effect in some cases for the intercalation of organic anions into the Mg_3/Al_1 LDH system. On the other hand, the substitution of magnesium by transition metals has negligible effect on the intercalation process. The synthesized and intercalated LDHs were characterized by X-ray diffraction (XRD) analysis, infrared (FTIR) spectroscopy, Raman spectroscopy, thermal (TG-DTG-DCS) analysis and scanning electron microscopy (SEM).

List of abbrevations

LDH	Layered Double Hydroxide
MMO	Mixed Metal Oxides
XRD	X ray diffraction
TGA	Thermogravimetric analysis
DSC	Differential scanning calorimetry
DTA	Differential Thermal Analysis
SEM	Scaning Electron Microscopy
FTIR	Fourier Transform Infrared

1. Introduction

Intercalation of layered double hydroxides (LDHs) with different anions is very attractive and important area, since the anion-exchange capacity can mostly be used to change chemical and physical properties of LDHs, such as the ion-exchange equilibrium (Miyata, 1983), ability to store and deliver biologically active materials (Khan and O'Hare, 2002), anion exchange kinetics (Nie, 2020) or anion exchange behaviour (Zhao et al., 2020). It was demonstrated that the combination of the lanthanide elements in the layers of LDHs, the luminescent materials with luminescence of cerium (IV) (Smalenskaite et al., 2017), europium (III) (Smalenskaite et al., 2018) or europium (II/III) (Sonoyama et al., 2020) could be obtained. Lanthanide doped LDH materials could be useful in many fields such as medicine (Sousa et al., 2006), fundamental investigations (Ferreira et al., 2012), catalysis (Jia et al., 2014), photochemistry (Fu et al., 2016), photomagnetoelectric devices (Wang et al., 2017) and biotechnological applications (Andrade et al., 2020). However, in many cases these LDHs are limited by the low emission intensity arising from the direct coordination of water molecules and hydroxyl groups to the lanthanide element centre in the layer. It was shown that intercalation of lanthanide-doped LDH materials with sensitizing anions (4-biphenylacetate (Gunawan and Xu, 2009), specific organic sensitizer (Liu et al., 2014), terephthalate (Smalenskaite et al., 2018, Smalenskaite et al., 2018)) allows to solve partially this problem. An efficient energy transfer between host and guest organic anions in the interlayer galleries influences the luminescence properties significantly.

Previously, Tran *et al.* (Tran et al., 2018, Lin et al., 2018) have intercalated LDHs with anions from amino, ethylenediaminetetraacetic, diethylenetriaminepentaacetic, citric, malic acids and other organic anions. They showed that these LDHs could be used as adsorbents to remove toxic metal cations and anions from aqueous media. Moreover, LDHs intercalated with anions from succinic acid and lauric acid were used as lubricant additives (Li et al., 2015). Dodecyl-sulfate-intercalated Mg/Al LDH nanosheets showed a high adsorption capability for the efficient and rapid removal of dyes (Lei et al., 2020). The intercalation of ciprofloxacin, a bactericidal antibiotic, into the interlayer space of LDHs was also performed (Cherif et al., 2020). Different release rates were observed depending on the intercalated structure, which were also influenced by the morphological characteristics. LDHs intercalated with anion containing nitrogen and sulphur (triazine-sulphonate) showed highly efficient flame retardant performance for polypropylene (Xu et al., 2020). The hexacyanoferrate-

* Corresponding author.
E-mail address: ligita.valeikiene@chgf.vu.lt (L. Valeikiene).

https://doi.org/10.1016/j.bioeco.2022.100024
Received 8 November 2021; Received in revised form 11 February 2022; Accepted 19 February 2022

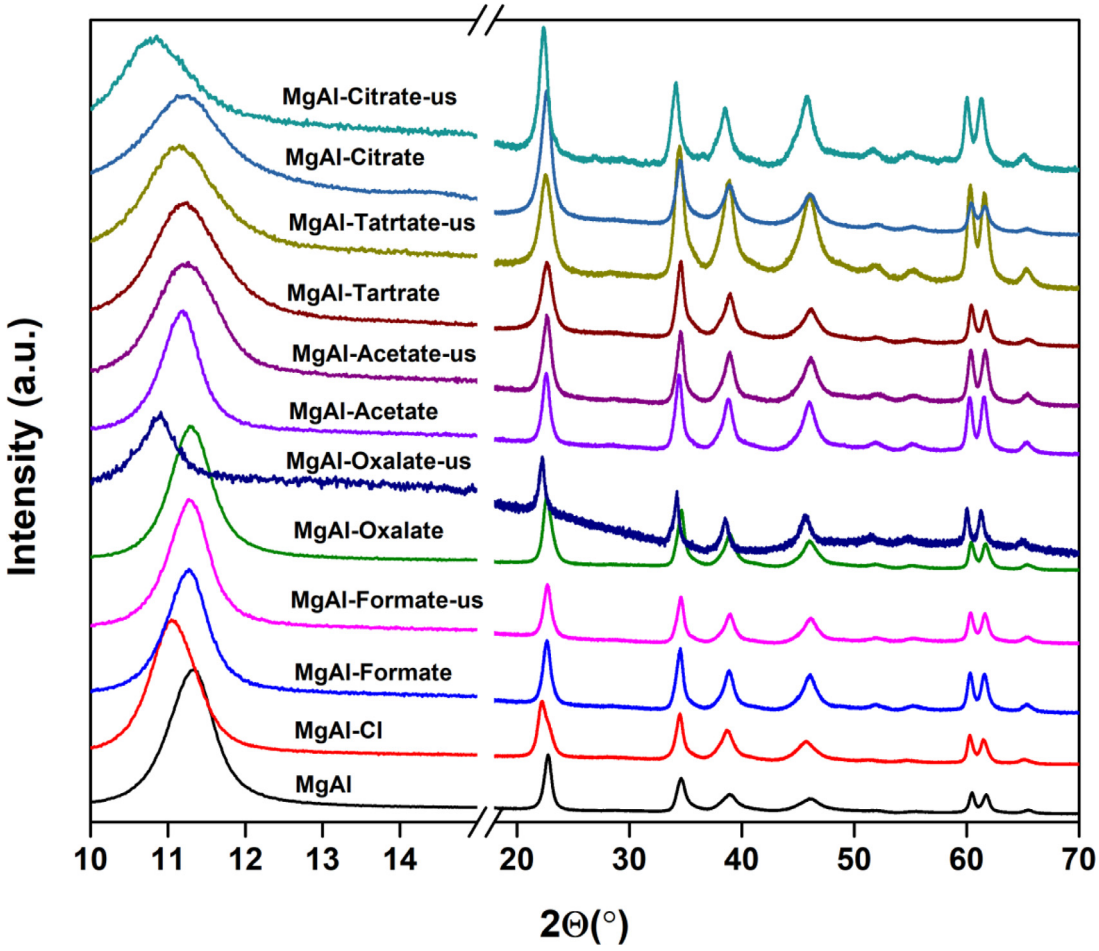

Fig. 1. XRD patterns of Mg_3/Al_1 LDHs with different intercalated anions and prepared without and with sonication (us).

intercalated LDHs were used for the detection of early-stage corrosion of steel (Wilhelm et al., 2020). LDHs with intercalated permanganate and peroxydisulphate anions were applied for the removal of chlorinated organic solvents from the contaminated water (Dietmann et al., 2020). The hypothesis that oxidising agents keep their properties after intercalation was confirmed. Besides, the applications of the LDHs in the context of new technologies of energy and nutrient recovery for the environment protection are also widely documented. Hybrid materials based on LDHs exhibit great potential in energy generation (Taviot-Gueho et al., 2018, Wang et al., 2020). Due to their unique physicochemical properties, transition metal-based LDHs are increasingly popular in the field of photo(electro)chemical water splitting for efficient and stable electrocatalysis for oxygen evolution reaction (Gao et al., 2021, Zheng et al., 2021, Bian et al., 2021). The LDHs composites with TiO_2 were also developed as adsorption-photocatalysis composite materials for water treatment (Suh et al., 2019). Additionally, the LDHs can be used for agricultural purposes after phosphate remediation applications (Buates and Imai, 2021, Zohar and Forano, 2021).

Recently, we investigated the influence of the origin of organic anion (oxalate, laurate, malonate, succinate, tartrate, benzoate, 1,3,5-benzentricarboxylate, 4-methylbenzoate, 4-dimethylaminobenzoate and 4-biphenylacetonate on the evolution of the chemical composition of the inorganic–organic LDHs system and on the luminescence properties of the Eu^{3+} doped LDHs containing these organic anions (Smalenskaite et al., 2019). The X-ray diffraction analysis results showed that the positions of diffraction peaks (003) of LDHs intercalated with anions were shifted to lower 2θ angle values in the XRD patterns. It is interesting to note, that the peaks of the diffractions of intercalated with different organic anions of Eu^{3+}-substituted LDHs was less pronounced in comparison with the samples without europium. Finally, it was concluded that depending on the size these anions could have specific vertical or horizontal orientations in the LDH structure. Moreover, intercalation chemistry of LDH materials and the advantages, disadvantages, and application possibilities of anion intercalated LDHs have been briefly summarized in (Ogino et al., 2020, Mallakpour et al., 2020). Recently our study on the transition metal substitution effects in $Mg_{3-x}M_x/Al_1$ (M = Mn, Co, Ni, Cu, Zn) LDHs synthesized using the same sol-gel chemistry approach has been published (Valeikiene et al., 2019). In the current investigation the results of further research exploring the ion exchange peculiarities in Mg_3/Al_1 and $Mg_{3-x}M_x/Al_1$ (M = Mn, Co, Ni, Cu, Zn) LDHs are presented. In this study the influence of ultrasound and cation substitution (Mn, Co, Ni, Cu, Zn) on the intercalation of organic anions (formate ($HCOO^-$), acetate (CH_3COO^-), oxalate ($C_2O_4^{2-}$), tartrate ($C_4H_6O_4^{2-}$) and citrate ($C_6H_5O_7^{3-}$)) to the Mg_3/Al_1 LDH structure for the first time has been investigated.

2. Experimental

Aluminium nitrate nonahydrate ($Al(NO_3)_3$•$9H_2O$, 98,5%, Chempur), magnesium nitrate hexahydrate ($Mg(NO_3)_2$•$6H_2O$), 99,0%, Chempur), manganese nitrate tetrahydrate ($Mn(NO_3)_2$•$4H_2O$, 98,0%, Chempur), cobalt nitrate hexahydrate ($Co(NO_3)_2$•$6H_2O$, 99%, Chempur), nickel nitrate hexahydrate ($Ni(NO_3)_2$•$6H_2O$, 98,0%, Chempur), copper nitrate trihydrate ($Cu(NO_3)_2$•$3H_2O$, 99,0%, Chempur) and zinc nitrate hexahy-

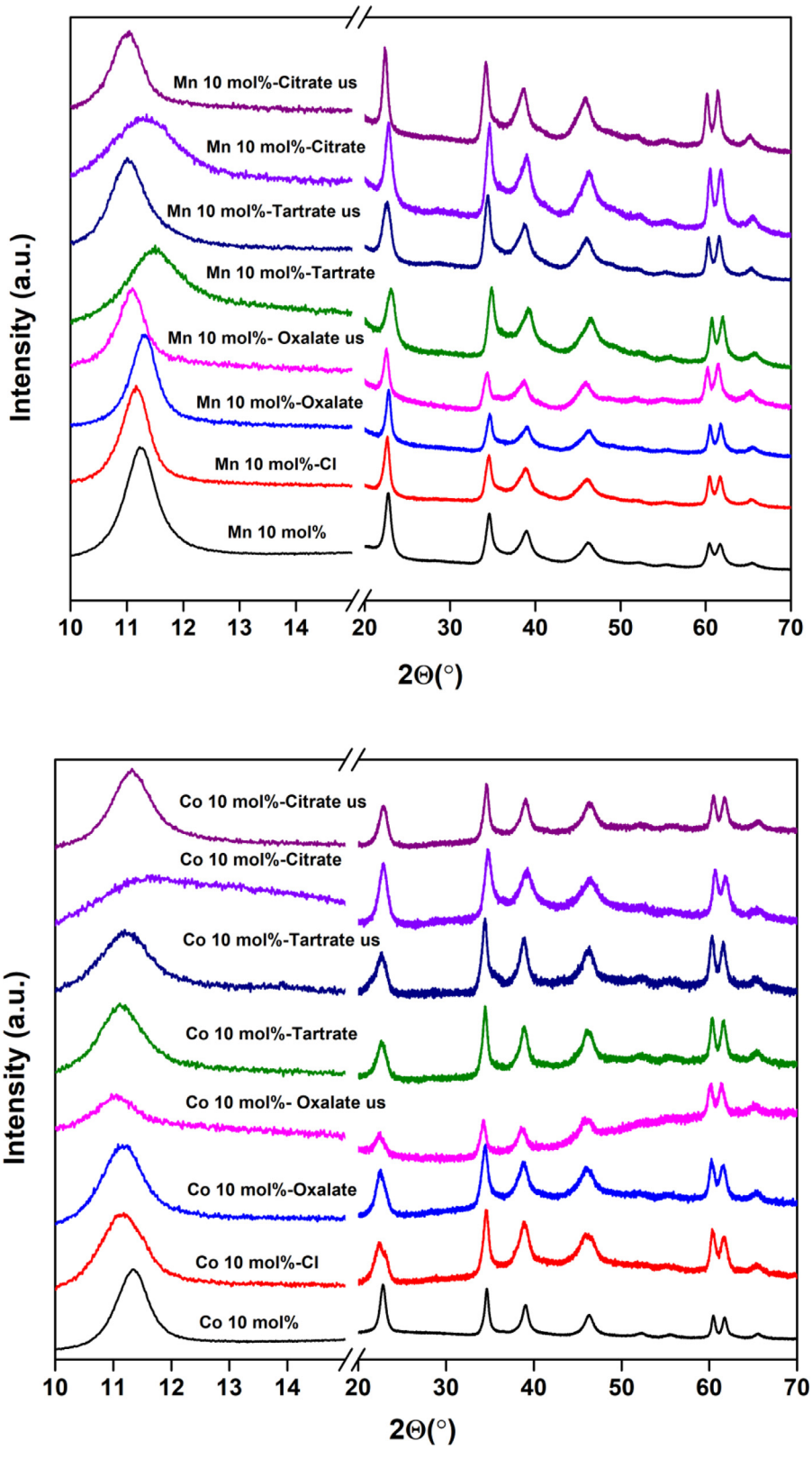

Fig. 2. XRD patterns of $Mg_{3-x}Mn_x/Al_1$ (top) and $Mg_{3-x}Co_x/Al_1$ (bottom) LDHs intercalated with different anions and prepared without and with sonication (us).

drate ($Zn(NO_3)_2$•$6H_2O$, 99,0%, Chempur) were used as starting materials in the preparation of Mg_3/Al_1 and transition metal substituted $Mg_{3-x}M_x/Al_1$ (M = Mn, Co, Ni, Cu, Zn) LDHs. Citric acid monohydrate ($C_6H_8O_7$•H_2O, 99,5%, Chempur) and 1,2-ethanediol ($C_2H_6O_2$, 99,8%, Chempur) were used as complexing agents in the sol-gel processing. Sodium chloride (NaCl, 99,5%, Chempur), hydrochloric acid (HCl, 37%, Sigma-Aldrich), sodium formate (HCO_2Na), 98,0%, Alfa Aesar), ammonium oxalate monohydrate ($(NH_4)_2C_2O_4$•H_2O, 99,8% Chempur), sodium acetate trihydrate (CH_3COONa•$3H_2O$), 99,0%, Chempur), potassium sodium tartrate tetrahydrate ($C_4H_4KNaO_6$•$4H_2O$, 99,0%, Chempur) and sodium citrate dihydrate ($C_6H_5O_7Na_3$•$2H_2O$, 99,0%, Chempur) were used for the intercalation of anions.

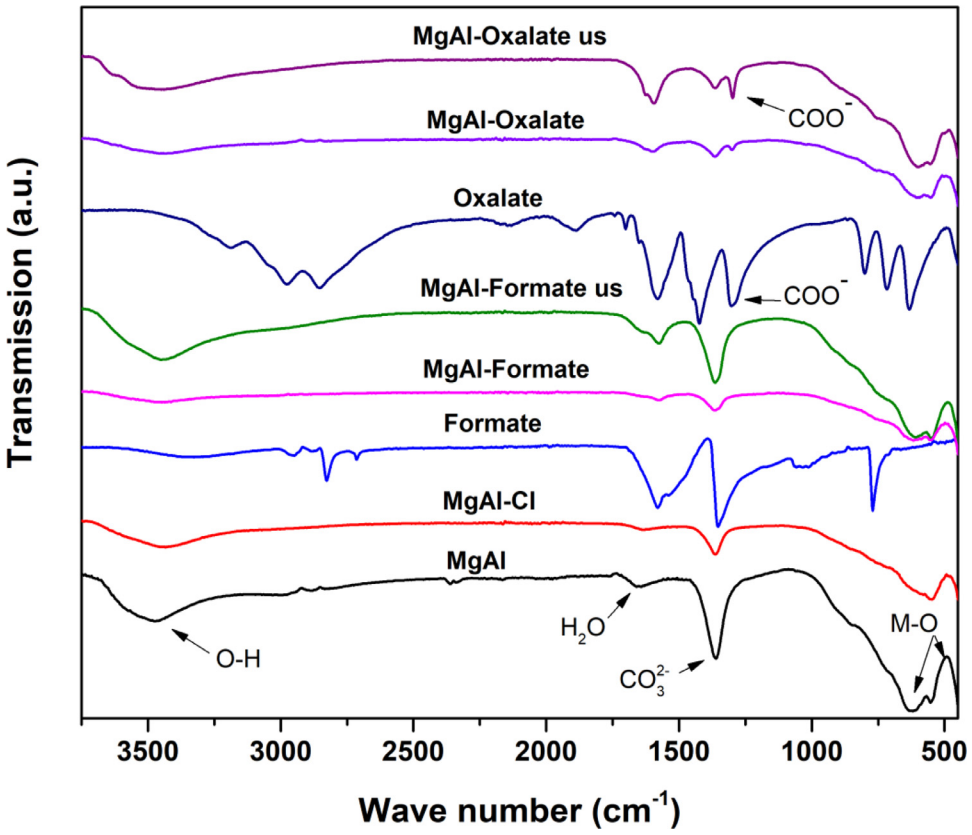

Fig. 3. FT-IR spectra of Mg_3/Al_1, Mg_3/Al_1-Cl, Mg_3/Al_1-formate, Mg_3/Al_1-oxalate LDHs and appropriate organic compounds used in ion exchange method.

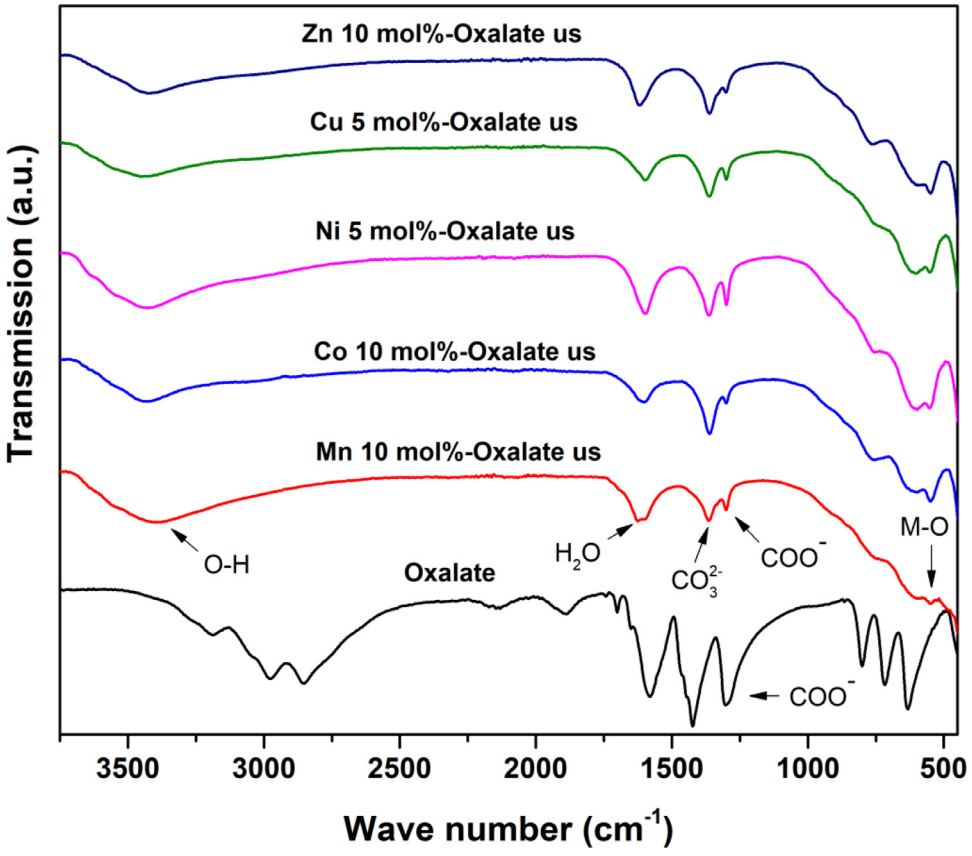

Fig. 4. FT-IR spectra of $Mg_{3-x}M_x/Al_1$ (M = Mn, Co, Ni, Cu and Zn) LDHs intercalated with oxalate using sonication (us) and appropriate organic compound used in ion exchange method.

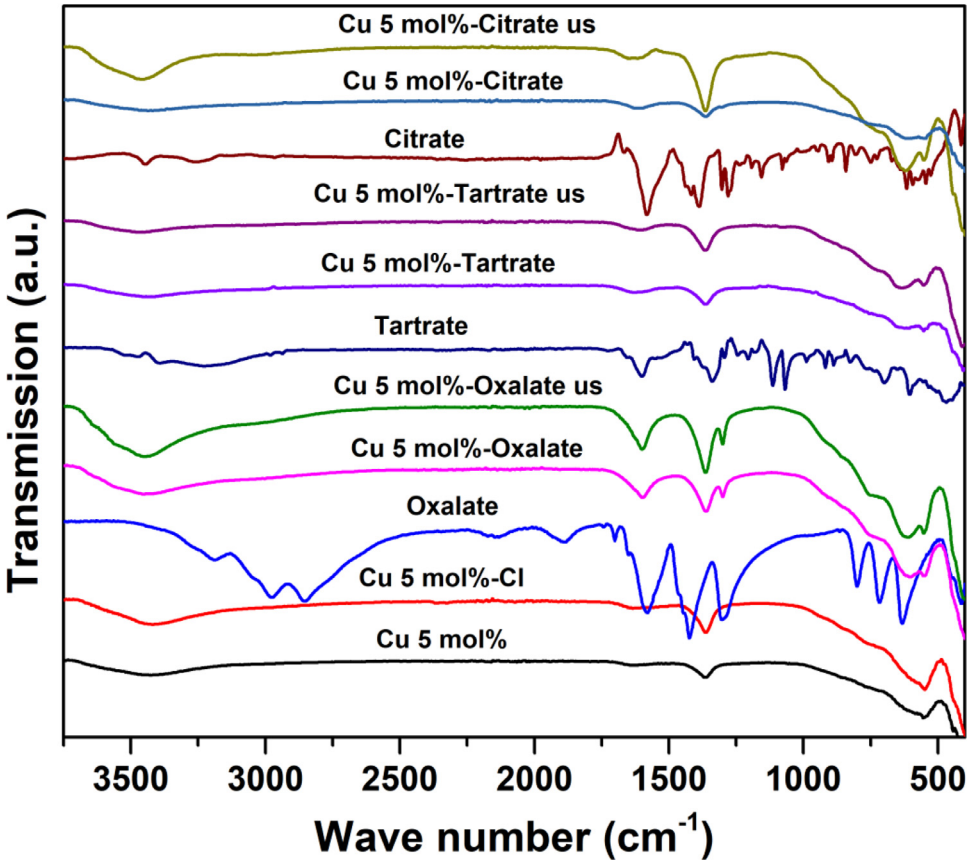

Fig. 5. FT-IR spectra of $Mg_{3-x}Cu_x/Al_1$ LDHs intercalated with oxalate, tartrate, citrate without and using sonication (us) and appropriate organic compounds used in ion exchange method.

For the synthesis of Mg_3/Al_1 and $Mg_{3-x}M_x/Al_1$ (M = Mn, Co, Ni, Cu, Zn) layered double hydroxides the stoichiometric amounts of starting materials were dissolved in distilled water under continuous stirring. Citric acid was added to the above solution and the obtained mixture was stirred for 1 h at 80°C. The 2 ml of 1,2-ethanediol was then added to the resulting solution with continuous stirring at 150°C until evaporation of the solvent. The obtained precursor gels were dried at 105 °C for 24 h. The mixed metal oxides (MMO) were synthesized by heating gels at 650 °C for 4 h. The Mg_3/Al_1 and $Mg_{3-x}M_x/Al_1$ (M = Mn, Co, Ni, Cu, Zn) LDHs were produced by reconstruction of LDH from MMO in deionized water at 50°C for 6 h under stirring.

Mg_3/Al_1 and $Mg_{3-x}M_x/Al_1$ (M = Mn, Co, Ni, Cu, Zn) -formate, -oxalate, -acetate, -tartrate and -citrate LDHs were synthesized using ion exchange method. Since the LDHs containing chloride anion are the most suitable precursors for the anion-exchange process (Smalenskaite et al., 2019, Gomez et al., 2020), the intercalation of organic anions formate, oxalate, acetate, tartrate and citrate in the Mg_3/Al_1 LDHs was performed from chloride containing LDHs. 0.5 g of Mg_3/Al_1 (or $Mg_{3-x}M_x/Al_1$ (M = Mn, Co, Ni, Cu, Zn)) LDH was added into 500 mL of a 1 M NaCl solution containing 3.3 mM of HCl. The resultant mixture was stirred for 24 h at room temperature. The suspension was filtered, the resultant solid washed with decarbonated water and acetone for several times and dried at 40°C for 24h. At the next step, 2 mmol of Mg_3Al_1 (or $Mg_{3-x}M_x/Al_1$ (M = Mn, Co, Ni, Cu, Zn)) was added in the solution of organic anions listed above taking 1.5 molar excess in comparison to LDHs. The reaction was carried out under two different methods: (a) the mixture was mixed at room temperature for 24 h; and (b) the mixture was sonicated at room temperature for 30 min. The suspension was filtered, the resultant solid washed with decarbonated water, acetone for several times and dried at 40°C for 24h.

For the characterization of phase purity of synthesized materials the X-ray diffraction (XRD) analysis was performed using a MiniFlex II diffractometer (Rigaku) (Cu Kα_1 radiation) in the 2θ range from 10 to 70° (step size of 0.02°) with the exposition time of 2 min per step. The lattice parameters of synthesized LDHs samples were also calculated according to the formula $c = 3/2[d(003) + 2d(006)]$, $a = 2d(110)$; here d is the basal spacing. Fourier transform infrared (FTIR) and Raman scattering spectra were recorded to explore the effect of ion exchange on the vibrational bands of pristine Mg_3/Al_1 and $Mg_{3-x}M_x/Al_1$ (M = Mn, Co, Ni, Cu, Zn) LDHs. The Fourier transform infrared (FT-IR) spectra were collected using an Alpha (Bruker, Inc., Germany) spectrometer. All spectra were recorded at ambient temperature in the range of 3750-480 cm^{-1}. Raman scattering spectra were measured with combined Raman and SNOM microscope Alpha 300 RS (WiTec, Germany) with 532 nm excitation laser source and 20x objective.The morphology of particles was investigated using a scanning electron microscope (SEM) Hitachi SU-70. The thermal decomposition of the synthesized materials was analyzed through thermogravimetric analysis and differential scanning calorimetry (TGA/DSC) using a simultaneous thermal analyzer 6000 (Perkin-Elmer) in air atmosphere at scan rate of 5°C/min and the temperature range from 30°C up to 700°C.

3. Results and discussion

The XRD patterns of the LDH phases obtained by the anion exchange reactions without or with usage of ultrasound (us) are shown in Fig. 1. As seen, the diffraction peaks for Mg_3/Al_1-Cl, Mg_3/Al_1-oxalate-us, Mg_3/Al_1-tartrate-us and Mg_3/Al_1-citrate-us are shifted to the lower values of 2θ angle indicating a considerable increase in the basal spacing c values as compared with the respective values for the main Mg_3/Al_1 LDH. These results clearly show that the treatment with ultrasound promotes the anion-exchange reactions significantly. This might be associated with increased reaction rate at such conditions (Sokol et al., 2019).

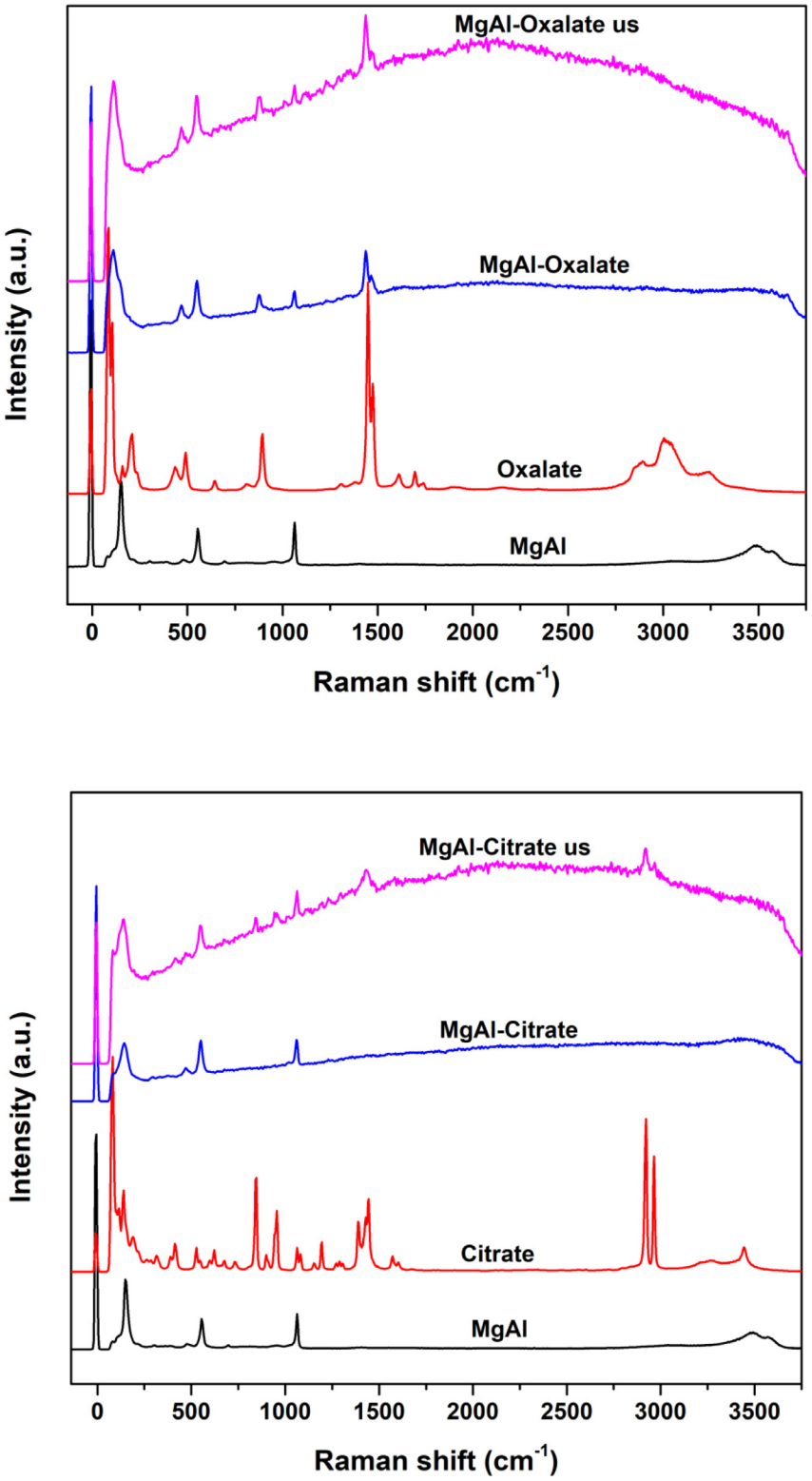

Fig. 6. Raman spectra of Mg_3/Al_1 and Mg_3/Al_1 LDHs intercalated with oxalate (top), citrate (bottom) anions without and under sonication (us) and appropriate organic compounds used in ion exchange method.

On the other hand, the positions of diffraction peaks (003) of Mg_3/Al_1-formate-us and Mg_3/Al_1-acetate-us LDHs are not shifted.

The lattice parameters of synthesized LDHs samples are summarized in Table 1. It is known that the lattice parameter *c* depends on the size, charge and orientation of the intercalated species. Thus, the results presented in Table 1 clearly shows that intercalation of chloride and oxalate, tartrate, citrate anion performed under ultrasound effect evidently occurs. Therefore, investigating the influence of nature of substituting transition metals on the character of anion-exchange reactions these four anions have been mostly applied.

The different manganese and cobalt substitution effects on the intercalation of above mentioned anions in $Mg_{3-x}Mn_x/Al_1$ and $Mg_{3-x}Co_x/Al_1$ LDHs could be observed in Fig. 2 and Tables 2 and 3. As seen from these results, the manganese has no influence on the intercalation

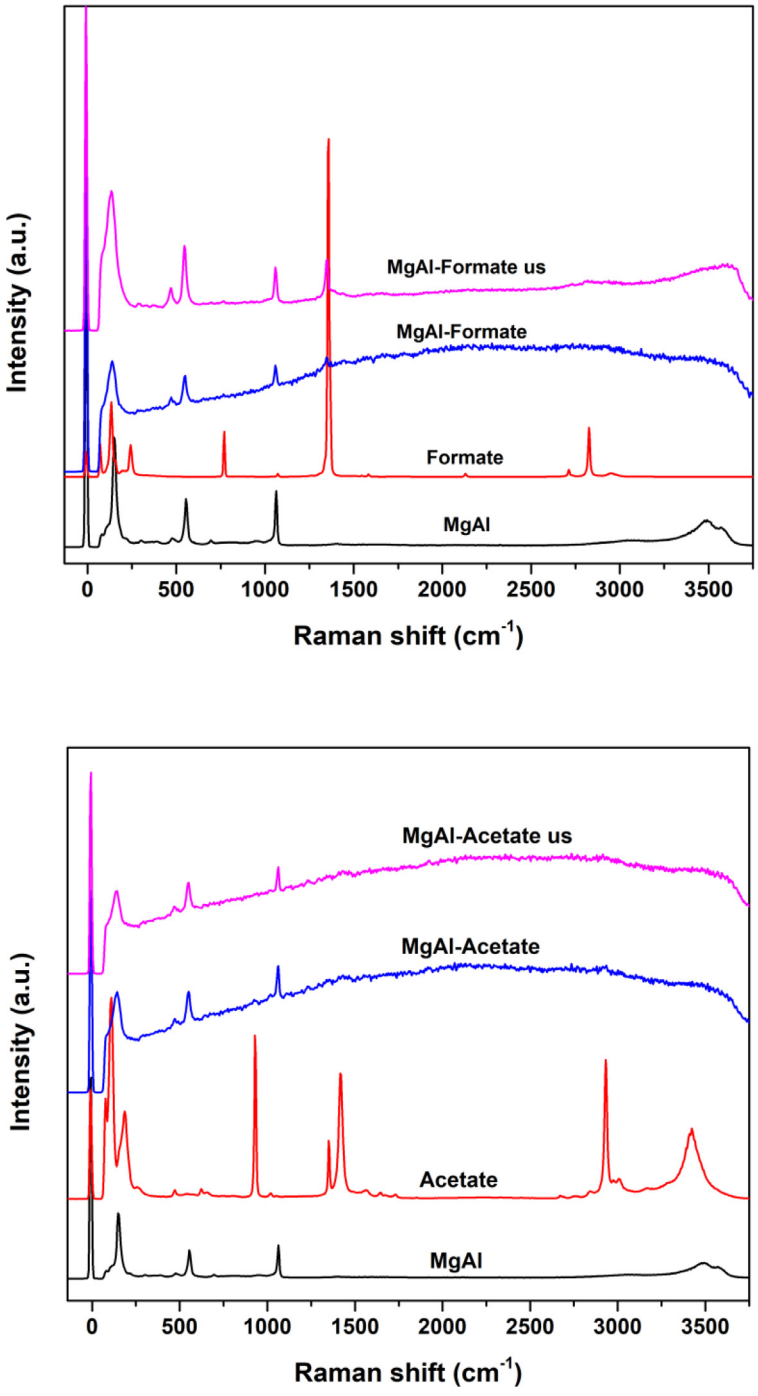

Fig. 7. Raman spectra of Mg_3/Al_1 and Mg_3/Al_1 LDHs intercalated with formate (top), acetate (bottom) anions without and under sonication (us) and appropriate organic compounds used in ion exchange method.

process. The shift of diffraction peaks attributable only to the sonicated $Mg_{3-x}Mn_x/Al_1$-anion-us LDH samples is visible. However, the different situation is happening in the case of cobalt substitution. The XRD results confirm that cobalt promotes intercalation of oxalate and tartrate to the interlayer of $Mg_{3-x}Co_x/Al_1$ LDHs without additional sonication.

It is interesting to note, that if ultrasound is not used the oxalate does not enter the interlayer of $Mg_{3-x}Ni_x/Al_1$ LDHs, but could be intercalated to the structure of $Mg_{3-x}Cu_x/Al_1$ LDHs (XRD results are presented in Fig. S1 and Tables 4-5). The behaviour of tartrate in these two nickel and copper substituted LDHs is completely opposite. The tartrate participates in the anion exchange reaction in $Mg_{3-x}Cu_x/Al_1$ LDHs, and does not enter the structure of $Mg_{3-x}Ni_x/Al_1$ LDHs. The similar shift of diffraction peaks as in $Mg_{3-x}Mn_x/Al_1$ was observed and in $Mg_{3-x}Zn_x/Al_1$ LDHs confirming that these anions could be intercalated to the zinc-substituted LDHs only under sonication (XRD results of $Mg_{3-x}Zn_x/Al_1$ LDHs are presented in Fig. S1 and Table 6). The origin of different behaviour of transition metals during the anion exchange reactions in LDHs is not clear yet. On the other hand, the used cations have different stable valence states. For example, the Mn, and Co may have several stable valence states, while the main valence state for Ni, Cu and Zn is +2. Thus, during the aliovalent substitution of divalent Mg in LDHs, the formation of oxygen vacancies to achieve neutrality should be also taking into account. Despite the substitution of magnesium by transition metals had only negligible effect on the intercalation process, these issues should be answered in the separate study.

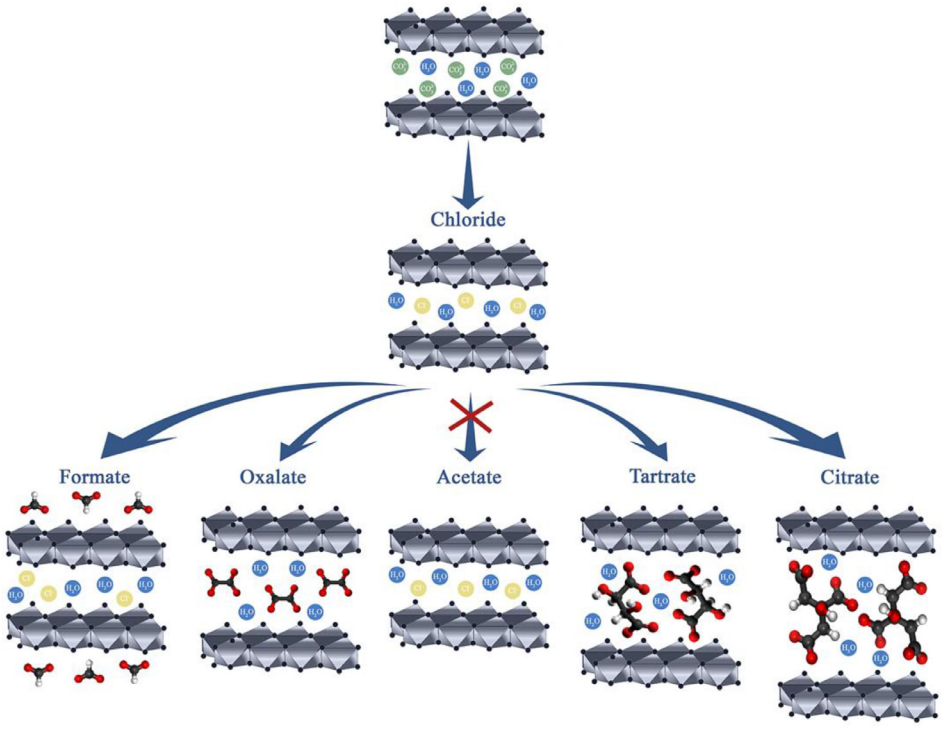

Fig. 8. The schematic representation of possible interaction of Mg_3/Al_1 LDHs with organic anions.

Table 1
Lattice parameters of Mg_3/Al_1 LDHs intercalated with different anions.

Sample	d (003), Å	d (006), Å	d (110), Å	Lattice parameters (Å)	
				a	*c*
Mg_3/Al_1	7.802	3.906	1.530	3.060(2)	23.422(4)
Mg_3/Al_1-Cl	8.009	3.993	1.535	3.071(3)	23.995(2)
Mg_3/Al_1-Formate	7.842	3.920	1.533	3.066(2)	23.524(4)
Mg_3/Al_1-Formate-us	7.842	3.913	1.533	3.066(1)	23.503(3)
Mg_3/Al_1-Acetate	7.901	3.925	1.536	3.072(2)	23.627(2)
Mg_3/Al_1-Acetate-us	7.900	3.928	1.533	3.066(2)	23.635(3)
Mg_3/Al_1-Oxalate	7.844	3.926	1.532	3.065(3)	23.546(1)
Mg_3/Al_1-Oxalate-us	8.097	3.997	1.541	3.082(3)	24.139(4)
Mg_3/Al_1-Tartrate	7.875	3.928	1.532	3.065(1)	23.599(2)
Mg_3/Al_1-Tartrate-us	7.934	3.951	1.534	3.068(2)	23.756(3)
Mg_3/Al_1-Citrate	7.913	3.928	1.532	3.065(2)	23.655(3)
Mg_3/Al_1-Citrate-us	8.153	3.969	1.541	3.081(3)	24.137(1)

Table 2
Lattice parameters of $Mg_{3-x}Mn_x/Al_1$ LDHs intercalated with different anions.

Sample	d (003), Å	d (006), Å	d (110), Å	Lattice parameters (Å)	
				a	*c*
Mn 10 mol%	7.875	3.908	1.532	3.064(1)	23.539(2)
Mn 10 mol% - Cl	7.926	3.926	1.532	3.065(1)	23.668(2)
Mn 10 mol% - Oxalate	7.816	3.903	1.530	3.061(3)	23.434(2)
Mn 10 mol% - Oxalate us	7.970	3.945	1.537	3.075(2)	23.791(4)
Mn 10 mol% - Tartrate	7.694	3.859	1.525	3.051(1)	23.120(2)
Mn 10 mol% - Tartrate us	8.037	3.941	1.534	3.069(2)	23.881(3)
Mn 10 mol% - Citrate	7.793	3.905	1.529	3.059(3)	23.408(4)
Mn 10 mol% - Citrate us	8.011	3.981	1.538	3.077(3)	23.962(3)

Table 3
Lattice parameters of $Mg_{3-x}Co_x/Al_1$ LDHs intercalated with different anions.

Sample	d (003), Å	d (006), Å	d (110), Å	Lattice parameters (Å)	
				a	*c*
Co 10 mol%	7.790	3.895	1.529	3.059(1)	23.371(3)
Co 10 mol% - Cl	7.916	3.965	1.534	3.068(2)	23.772(2)
Co 10 mol% - Oxalate	7.920	3.943	1.534	3.069(2)	23.712(4)
Co 10 mol% - Oxalate us	8.062	3.986	1.537	3.075(1)	24.052(4)
Co 10 mol% - Tartrate	7.898	3.919	1.533	3.066(2)	23.607(4)
Co 10 mol% - Tartrate us	7.956	3.929	1.533	3.067(3)	23.721(2)
Co 10 mol% - Citrate	7.685	3.885	1.526	3.052(3)	23.185(3)
Co 10 mol% - Citrate us	7.810	3.884	1.529	3.059(2)	23.370(2)

Table 4
Lattice parameters of $Mg_{3-x}Ni_x/Al_1$ LDHs intercalated with different anions.

Sample	d (003), Å	d (006), Å	d (110), Å	Lattice parameters (Å)	
				a	c
Ni 5 mol%	7.865	3.923	1.533	3.066(2)	23.567(2)
Ni 5 mol% - Cl	7.763	3.858	1.526	3.053(1)	23.221(2)
Ni 5 mol% - Oxalate	7.792	3.915	1.529	3.059(2)	23.435(4)
Ni 5 mol% - Oxalate us	8.140	3.993	1.539	3.079(1)	24.192(2)
Ni 5 mol% - Tartrate	7.961	3.966	1.533	3.067(2)	23.840(3)
Ni 5 mol% - Tartrate us	8.042	3.949	1.535	3.071(3)	23.913(3)
Ni 5 mol% - Citrate	7.897	3.900	1.530	3.061(2)	23.546(3)
Ni 5 mol% - Citrate us	7.960	3.945	1.534	3.068(2)	23.777(1)

The FT-IR spectra recorded for all LDH samples are very similar to each other with negligible differences. The FT-IR results in some of the cases confirmed the obtained XRD results concerning the anion exchange processes Fig. 3. shows FT-IR spectra of Mg_3/Al_1-oxalate and Mg_3/Al_1-formate LDHs along with appropriate organic salts. As seen, FT-IR spectra of Mg_3/Al_1 and Mg_3/Al_1-Cl LDH samples in the region of 3750-480 cm^{-1} contain the absorption bands at about 3600-3100 cm^{-1} and weaker bands at 1655-1640 cm^{-1} which could be attributed to the stretch vibration in (-OH) groups originated from the hydroxyl layers and from intercalated water molecules (Smalenskaite et al., 2017, Smalenskaite et al., 2019, Gomez et al., 2020, Liu et al., 2014, Sokol et al., 2018). The strong absorption bands visible at 1360 cm^{-1} are attributed to the asymmetric vibration modes of ionic carbonate (CO_3^{2-}), which still exists in the interlayer of LDHs. The FT-IR spectra of Mg_3/Al_1-formate and Mg_3/Al_1-formate-us LDHs qualitatively cannot be distinguished from the spectrum of Mg_3/Al_1 LDH. Moreover, no specific

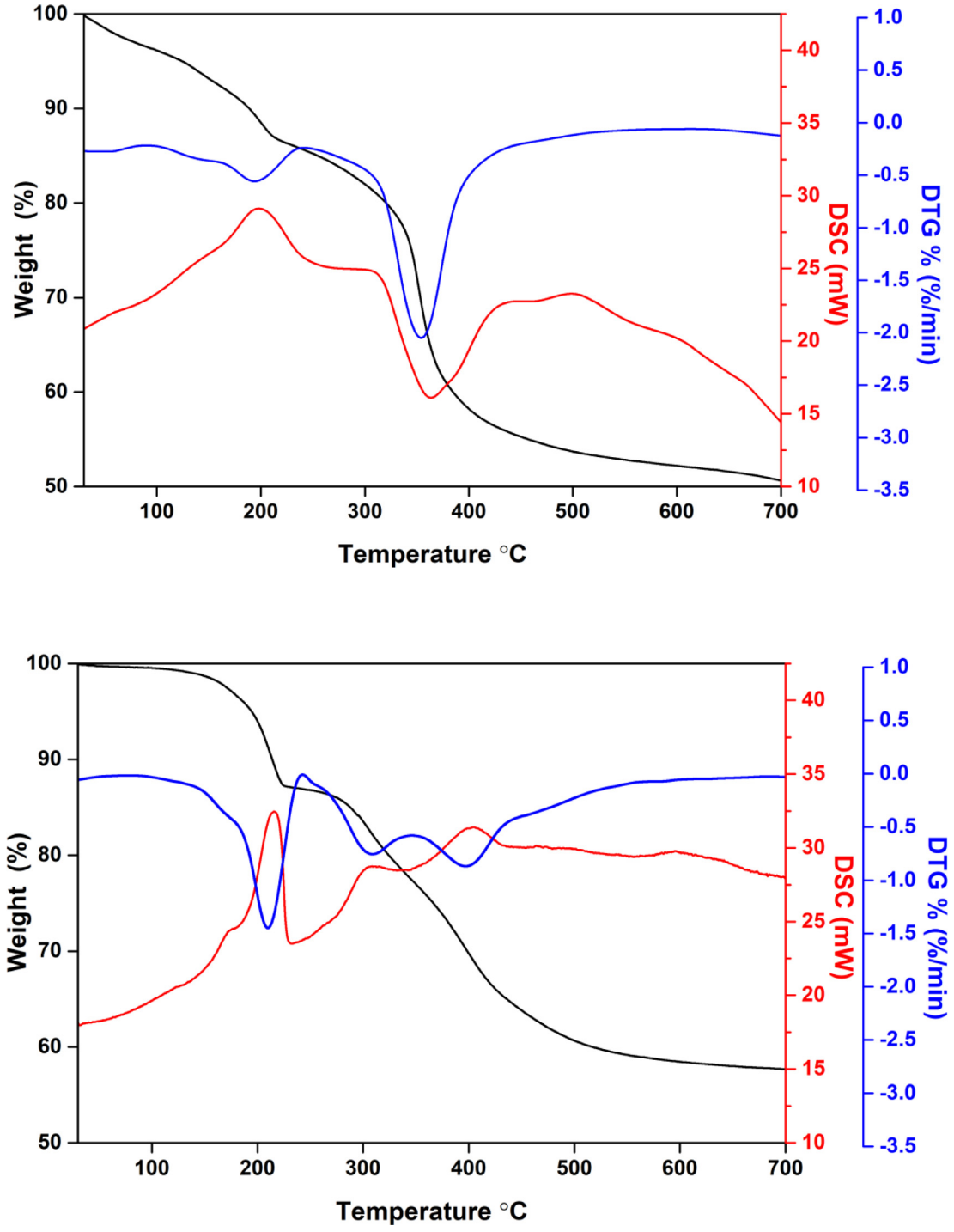

Fig. 9. TG-DTG-DCS curves of Mg_3Al_1 (bottom) and Mg_3Al_1 LDHs intercalated with citrate under sonication (top).

absorption bands attributable to the sodium formate are seen in these FT-IR spectra. However, the FT-IR spectra of Mg_3/Al_1 LDHs intercalated with oxalate ion contain the strong absorption band at 1315 cm^{-1} which is assigned as symmetric (-COO^-) vibration in the oxalate groups.

FT-IR spectra of $Mg_{3-x}M_x/Al_1$ (M = Mn, Co, Ni, Cu and Zn) LDHs intercalated with oxalate using sonication are shown in Fig. 4. All spectra independent on the used transition metal for substitution confirms intercalation of oxalate to the structure of LDHs as was determined by XRD analysis. On the other hand, the FT-IR spectroscopy results do not support fully the conclusion that the tartrate anion participates in the anion exchange reaction in $Mg_{3-x}Cu_x/Al_1$ LDHs (see Fig. 5). Only few characteristic absorption bands of tartrate were observed in the FT-IR spectra of $Mg_{3-x}Cu_x/Al_1$-tartrate and $Mg_{3-x}Cu_x/Al_1$-tartrate-us LDHs.

The Raman spectroscopy provides molecular level information on short range structure or local symmetry which is difficult to acquire by other structure-sensitive techniques (Malakauskaite-Petruleviciene et al., 2015, Blasiak et al., 2017) Fig. 6. compares Raman spectra of oxalate, citrate, Mg_3/Al_1 and Mg_3/Al_1 LDHs intercalated with oxalate and citrate anions and obtained without and under sonification conditions. The strong high frequency features located at about 1500 cm^{-1} for oxalate (symmetry D_{2h}) (Peterson and Pullman, 2016) are vis-

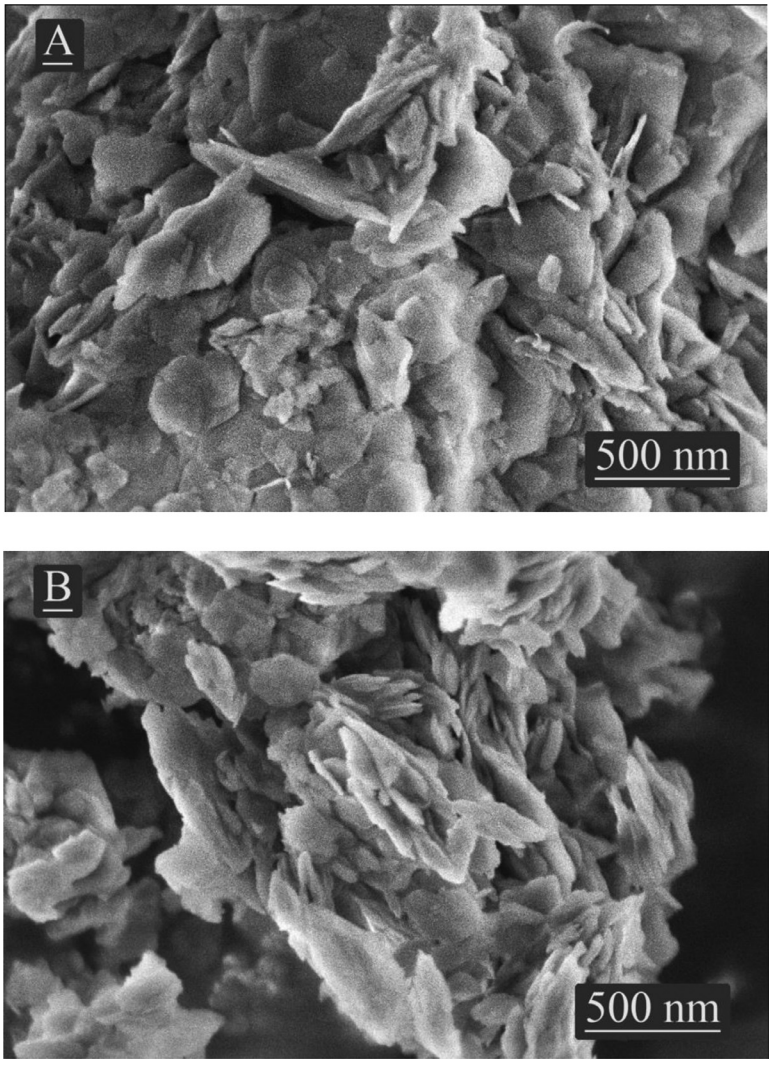

Fig. 10. SEM micrographs of Mg_3Al_1 LDHs intercalated with formate without (A) and under sonication (B).

Table 5
Lattice parameters of $Mg_{3-x}Cu_x/Al_1$ LDHs intercalated with different anions.

Sample	d (003), Å	d (006), Å	d (110), Å	Lattice parameters (Å)	
				a	c
Cu 5 mol%	7.785	3.903	1.531	3.062(3)	23.387(3)
Cu 5 mol% - Cl	7.842	3.909	1.531	3.062(3)	23.490(3)
Cu 5 mol% - Oxalate	7.994	3.950	1.537	3.074(2)	23.843(3)
Cu 5 mol% - Oxalate us	8.054	3.959	1.537	3.074(1)	23.959(4)
Cu 5 mol% - Tartrate	7.701	3.860	1.527	3.054(2)	23.134(2)
Cu 5 mol% - Tartrate us	7.977	3.960	1.536	3.073(2)	23.849(2)
Cu 5 mol% - Citrate	7.838	3.910	1.532	3.064(1)	23.489(1)
Cu 5 mol% - Citrate us	7.934	3.916	1.534	3.069(1)	23.652(4)

Table 6
Lattice parameters of $Mg_{3-x}Zn_x/Al_1$ LDHs intercalated with different anions.

Sample	d (003), Å	d (006), Å	d (110), Å	Lattice parameters (Å)	
				a	c
Zn 10 mol%	7.734	3.849	1529	3.057(3)	23.147(4)
Zn 10 mol% - Cl	7.764	3.842	1.527	3.054(2)	23.173(3)
Zn 10 mol% - Oxalate	7.635	3.816	1.526	3.051(3)	22.902(2)
Zn 10 mol% - Oxalate us	7.788	3.886	1.529	3.059(2)	23.341(2)
Zn 10 mol% - Tartrate	7.704	3.853	1.531	3.062(2)	23.116(1)
Zn 10 mol% - Tartrate us	7.835	3.879	1.532	3.063(2)	23.389(4)
Zn 10 mol% - Citrate	7.854	3.908	1.533	3.066(1)	23.507(2)
Zn 10 mol% - Citrate us	7.892	3.894	1.532	3.065(1)	23.522(3)

ible in the Raman spectra of Mg_3/Al_1-oxalate and Mg_3/Al_1-oxalate-us LDHs. The well-defined characteristic bands of citrate (Tada et al., 2004) could be determined only in sonicated Mg_3/Al_1-citrate-us. These results are in a good agreement with previously discussed XRD and FT-IR results.

Different spectral patterns were observed for Mg_3/Al_1 LDHs intercalated with formate and acetate anions (Fig. 7). Interestingly, the main peak position observed for the formate (Su et al., 2005) could be detected also in the Raman spectra of Mg_3/Al_1 LDHs intercalated with formate. However, this feature was not confirmed by specific shift of the diffraction peaks in the XRD patterns of this compounds. On the other hand, it is clearly seen that Raman spectra of Mg_3/Al_1-acetate LDHs do not contain any specific absorption bands attributable to acetate (Noma et al., 1991).

Therefore it can be concluded that formate contrary oxalate and tartrate and citrate is only adsorbed on the surface of LDHs but does not enter the interlayer space (Fig. 8).

Moreover, the representative Raman spectra shown in Fig. S2 confirm that transition metal substitution in Mg_3/Al_1 LDHs supports intercalation of anions.

The TG-DTG-DCS curves of Mg_3/Al_1 and Mg_3/Al_1 LDHs intercalated with citrate under sonication are shown in Fig. 9. The initial mass loss observed in the temperature range of 30-210°C is associated with evolution of moisture and adsorbed water. The main decomposition of LDHs occurs via continuous mass loss step in the temperature range of 210-600°C. These thermal behaviour results from the loss of the coordinated

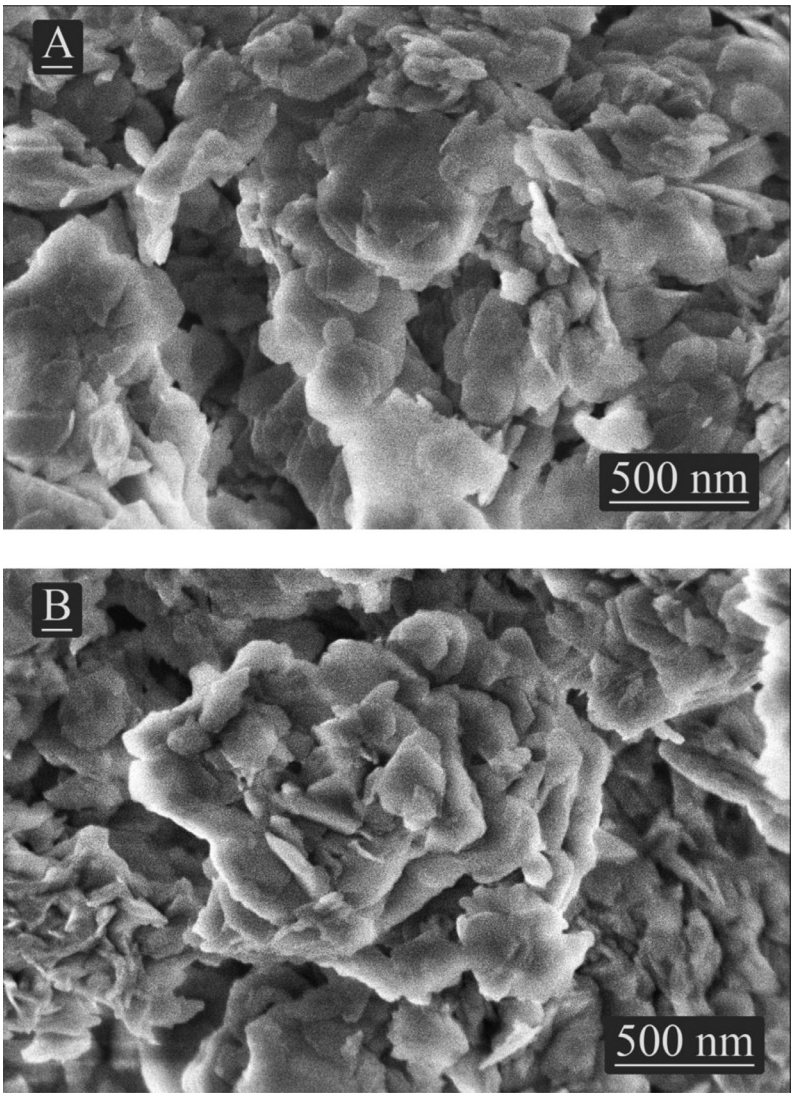

Fig. 11. SEM micrographs of Mg_3Al_1 LDHs intercalated with tartrate without (A) and under sonication (B).

water and the intercalated anions and dehydroxylation of the layers followed by collapse of the layered structure in the higher temperature range. It could be easily observed that the total mass loss for the Mg_3/Al_1 LDH sample is about 42.5%. The increased total loss (about 48.9%) observed for the Mg_3/Al_1-citrate-us LDHs confirms once again that organic anion is intercalated in the layered structure of LDH or/and adsorbed on the surface of synthesized material. The analogous TG results were observed for the Mg_3Al_1 LDHs intercalated with formate, tartrate and oxalate.

The morphology of the synthesized LDHs were examined using scanning electron microscopy. The characteristic feature of synthesized LDHs is the formation of plate-like particles with hexagonal shape (Xu and Braterman, 2010). It is interesting to note that the SEM images of sol-gel derived LDH samples were almost identical independent on the nature of anion used for the intercalation, on the selected transition metal for substitution and on the used intercalation procedure. The representative SEM micrographs for the Mg_3/Al_1 LDHs intercalated with formate without and under sonication are depicted in Fig. 10. As seen, the solids are composed of differently agglomerated plate-like particles with the size about of 500 nm. The agglomerates are slightly larger in the case of sonicated LDH-formate sample. The XRD, TG and Raman results of characterization of Mg_3/Al_1-formate LDHs supported the conclusion that formate anion is mostly adsorbed on the surface of LDHs.

The representative SEM micrographs of LDHs intercalated with tartrate anion which participated in anion exchange reaction are shown in Fig. 11. The surface microstructure still represents the characteristic features of LDHs without changes in the particle shape or size. Evidently, the surface microstructure of these LDH samples is mostly defined by the used sol-gel preparation technique.

4. Conclusions

The Mg_3/Al_1 and $Mg_{3-x}M_x/Al_1$ (M = Mn, Co, Ni, Cu, Zn) layered double hydroxides (LDHs) were synthesized using sol-gel synthesis technique and intercalated with different organic anions (formate ($HCOO^-$), acetate (CH_3COO^-), oxalate ($C_2O_4^{2-}$), tartrate ($C_4H_6O_4^{2-}$) and citrate ($C_6H_5O_7^{3-}$)) using ion exchange approach. The influence of ultrasound (us) and cation substitution on the intercalation of organic anions to the Mg_3/Al_1 LDH has been investigated. The XRD analysis results showed that the diffraction peaks for Mg_3/Al_1-Cl, Mg_3/Al_1-oxalate-us, Mg_3/Al_1-tartrate-us and Mg_3/Al_1-citrate-us were shifted to the lower values of 2θ angle indicating a considerable increase in the basal spacing c values as compared with the respective values for the main Mg_3/Al_1 LDH. These results confirmed that the treatment with ultrasound promotes the anion-exchange reactions. On the other hand, the positions of diffraction peaks (003) of Mg_3/Al_1-formate-us and Mg_3/Al_1-acetate-us LDHs were not shifted. From the Raman spectroscopy results it was concluded that

formate anion contrary oxalate, tartrate and citrate was only adsorbed on the surface of LDHs but did not participated in ion exchange reaction. The SEM images of sol-gel derived LDH samples were almost identical independent on the nature of anion used for the intercalation, on the selected transition metal for substitution and on the used intercalation procedure. Thus, the surface microstructure of these LDH samples was mostly defined by the used sol-gel preparation technique. Finally, the results indicated summarized in this study let us to conclude that ultrasound had a positive effect in some cases for the intercalation of organic anions into the Mg_3/Al_1 LDH system. On the other hand, the substitution of magnesium by transition metals had only negligible effect on the intercalation process.

Authors' contributions

L. Valeikiene: Synthesis, Characterisation, Investigation, Data curation, Visualization, Writing-Original draft preparation;

K.Kriukaite: Synthesis

I. Grigoraviciute - Puroniene: Supervision, Methodology, Reviewing and Editing.

A. Popov: Raman spectroscopy

A. Kareiva: Supervision, Methodology, Writing- Reviewing and Editing, Validation.

Supporting information

Fig. S1. XRD patterns of $Mg_{3-x}Ni_x/Al_1$ (top), $Mg_{3-x}Cu_x/Al_1$ (middle) and $Mg_{3-x}Zn_x/Al_1$ (bottom) LDHs with different intercalated organc anions and prepared without and with sonication (us).

Fig. S2. Raman spectra of Mg_3Al_1, $Mg_{3-x}Zn_xAl_1$ and $Mg_{3-x}Ni_xAl_1$ intercalated with oxalate (top), citrate (bottom) anions under sonication (us) and appropriate organic compound used in ion exchange method.

L.Valeikiene_Supplementary files

Declaration of Competing Interests

The authors declare that they have no known competing financial interests or personal relationships that could have appeared to influence the work reported in this paper.

The authors declare the following financial interests/personal relationships which may be considered as potential competing interests:

Supplementary materials

Supplementary material associated with this article can be found, in the online version, at doi:10.1016/j.bioeco.2022.100024.

CRediT authorship contribution statement

Ligita Valeikiene: Investigation, Data curation, Visualization, Writing – original draft. **Inga Grigoraviciute-Puroniene:** Supervision, Methodology. **Aivaras Kareiva:** Supervision, Methodology, Writing – review & editing, Validation.

References

Andrade, KN, Arizaga, GGC, Mayorga, JAR., 2020. Effect of Gd and Dy concentrations in layered double hydroxides on contrast in magnetic resonance imaging. Processes 8, 462.

Bian, XN, Zhang, S, Zhao, YX, Shi, R, Zhang, T., 2021. Layered double hydroxide-based photocatalytic materials toward renewable solar fuels production. Infomat 3, 719–738.

Blasiak, B, Londergan, CH, Webb, LJ, Cho, M., 2017. Vibrational probes: from small molecule solvatochromism theory and experiments to applications in complex systems. Accounts Chem. Res. 50, 968–976.

Buates, J, Imai, T., 2021. Application of biochar functionalized with layered double hydroxides: improved plant growth performance after use as phosphate adsorbent. Appl. Sci. 11, 6489.

Cherif, NF, Constantino, VRL, Hamdaoui, O, Leroux, F, Taviot-Gueho, C., 2020. New insights into two ciprofloxacin-intercalated arrangements for layered double hydroxide carrier materials. New J. Chem. 44, 10076–10086.

Dietmann, KM, Linke, T, Nogal Sanchez, MD, Perez Pavon, JL, Rives, V, 2020. Layered double hydroxides with intercalated permanganate and peroxydisulphate anions for oxidative removal of chlorinated organic solvents contaminated water. Minerals 10, 462.

Ferreira, RAS, Nolasco, M, Roma, AC, Longo, RL, Malta, OL, Carlos, LD., 2012. Dependence of the lifetime upon the excitation energy and intramolecular energy transfer rates: The 5D0 EuIII emission case. Chem. - A Eur. J. 18, 12130–12139.

Fu, Y, Ning, FY, Xu, SM, HL, An, Shao, MF, Wei, M., 2016. Terbium doped ZnCr-layered double hydroxides with largely enhanced visible light photocatalytic performance. J. Mater. Chem. A 4, 3907–3913.

Gao, R, Zhu, J, Yan, DP., 2021. Transition metal-based layered double hydroxides for photo(electro)chemical water splitting: a mini review. Nanoscale 13, 13593–13603.

Gomez, NAG, Silva, GM, Wilhelm, HM, Wypych, F., 2020. Zn_2Al layered double hydroxides intercalated with nitrate and p-aminobenzoate as ultraviolet protective agents in low-density polyethylene nanocomposites and natural insulating oils. J. Braz. Chem. Soc. 31, 971–981.

Gunawan, P, Xu, R., 2009. Lanthanide-doped layered double hydroxides intercalated with sensitizing anions: Efficient energy transfer between host and guest layers. J. Phys. Chem. C 113, 17206–17214.

Jia, YQ, Zhao, S, Song, YF., 2014. The application of spontaneous flocculation for the preparation of lanthanide-containing polyoxometalates intercalated layered double hydroxides: highly efficient heterogeneous catalysts for cyanosilylation. Appl. Catal A-Gener. 487, 172–180.

Khan, AI, O'Hare, D., 2002. Intercalation chemistry of layered double hydroxides: recent developments and applications recent developments and applications. J. Mater. Chem. 12, 3191–3198.

Lei, SQ, Wang, SN, Gao, BX, Zhan, YL, Zhao, QC, Jin, SS, Song, GX, Lyu, XC, Zhang, YH, Tang, Y., 2020. Ultrathin dodecyl-sulfate-intercalated Mg-Al layered double hydroxide nanosheets with high adsorption capability for dye pollution. J. Coll. Interf. Sci. 577, 181–190.

Li, S, Qin, H, Zuo, R, Bai, Z., 2015. Intercalation of methotrexatum into layered double hydroxides via exfoliation-reassembly process. Appl. Surf. Sci. 353, 643–650.

Lin, ST, Tran, HN, Chao, HP, Lee, JF., 2018. Layered double hydroxides intercalated with sulfur-containing organic solutes for efficient removal of cationic and oxyanionic metal ions. Appl. Clay Sci. 162, 443–453.

Liu, L, Wang, Q, Gao, C, Chen, H, Liu, W, Tang, Y., 2014. Dramatically enhanced luminescence of layered terbium hydroxides as induced by the synergistic effect of Gd3+ and organic sensitizers. J. Phys. Chem. C 118, 14511–14520.

Liu, L, Wang, Q, Gao, C, Chen, H, Liu, W, Tang, Y., 2014. Dramatically enhanced luminescence of layered terbium hydroxides as induced by the synergistic effect of Gd^{3+} and organic sensitizers. J. Phys. Chem. C 118, 14511–14520.

Malakauskaite-Petruleviciene, M, Stankeviciute, Z, Niaura, G, Prichodko, A, Kareiva, A, 2015. Synthesis and characterization of sol-gel derived calcium hydroxyapatite thin films spin-coated on silicon substrate. Ceram. Int. 41, 7421–7428.

Mallakpour, S, Hatami, M, Hussain, CM., 2020. Recent innovations in functionalized layered double hydroxides: fabrication, characterization, and industrial applications. Adv. Coll. Interf. Sci. 283, 102216.

Miyata, S., 1983. Anion-exchange properties of hydrotalcite-like compounds. Clays Clay Miner. 31, 305–311.

Nie, WY., 2020. Dynamics analysis of anion exchange in layered double hydroxides. Brazil J. Chem. Eng. 37, 795–803.

Noma, H, Miwa, Y, Yokoyama, I, Machida, K., 1991. Infrared and Raman intensity parameters of sodium acetate and their intensity distributions. J. Molec. Struct. 242, 207–219.

Ogino, I, Hirayama, Y, Mukai, SR., 2020. Intercalation chemistry and thermal characteristics of layered double hydroxides possessing organic phosphonates and sulfonates. New J. Chem. 44, 10002–10010.

Peterson, KI, Pullman, DP., 2016. Determining the structure of oxalate anion using infrared and Raman spectroscopy coupled with gaussian calculations. J. Chem. Educ. 93, 1130–1133.

Smalenskaite, A, Vieira, DEL, Salak, AN, Ferreira, MGS, Katelnikovas, A, Kareiva, A., 2017. A comparative study of co-precipitation and sol-gel synthetic approaches to fabricate cerium-substituted Mg-Al layered double hydroxides with luminescence properties. Appl. Clay Sci. 143, 175–183.

Smalenskaite, A, Sen, S, Salak, AN, Ferreira, MGS, Beganskiene, A, Kareiva, A., 2018. Sol-gel derived lanthanide-substituted layered double hydroxides $Mg_3/Al_{1-x}Ln_x$. Acta Physica Polonica A 133, 884–886.

Smalenskaite, A, Salak, AN, Kareiva, A., 2018. Induced neodymium luminescence in sol-gel derived layered double hydroxides. Mendeleev Commun. 28, 493–494.

Smalenskaite, A, Salak, AN, Ferreira, MGS, Skaudzius, R, Kareiva, A., 2018. Sol-gel synthesis and characterization of hybrid inorganic-organic Tb(III)-terephthalate containing layered double hydroxides. Opt. Mater. 80, 186–196.

Smalenskaite, A, Pavasaryte, L, Yang, TCK, Kareiva, A., 2019. Undoped and Eu^{3+} doped magnesium-aluminium layered double hydroxides: peculiarities of intercalation of organic anions and investigation of luminescence properties. Materials 12, 736.

Sokol, D, Salak, AN, Ferreira, MGS, Beganskiene, A, Kareiva, A., 2018. Bi-substituted $Mg_3Al\text{-}CO_3$ layered double hydroxides. J. Sol-Gel Sci. Technol. 85, 221–230.

Sokol, D, Vieira, D, Zarkov, A, Ferreira, M, Beganskiene, A, Rubanik, V, Shilin, A, Kareiva, A, Salak, A., 2019. Sonication accelerated formation of Mg-Al-phosphate layered double hydroxide via sol-gel prepared mixed metal oxides. Scient Reports 9, 10419.

Sonoyama, N, Takagi, K, Yoshida, S, Ota, T, Kimilita, PD, Ogasawara, Y., 2020. Optical properties of the europium (II) and (III) ions doped metal oxides obtained from sintering layered double hydroxides, and their fine structures. Appl. Clay Sci. 186, 105440.

Sousa, FL, Pillinger, M, Ferreira, RAS, Granadeiro, CM, Cavaleiro, AMV, Rocha, J, Carlos, LD, Trindade, T, Nogueira, HIS., 2006. Luminescent polyoxotungstoeuropate anion-pillared layered double hydroxides. Eur. J. Inorg. Chem. 726–734.

Su, J, Yu, XL, You, JL, Yin, ST, 2005. Raman spectroscopy studies on the aqueous solutions of sodium formate and lithium formate. Guang Pu Xue Yu Guang Pu Fen Xi 25, 532–536.

Suh, MJ, Shen, Y, Chan, CK, Kim, JH., 2019. Titanium Dioxide-Layered Double Hydroxide Composite Material for Adsorption-Photocatalysis of Water Pollutants. Langmuir 35, 8699–8708.

Tada, H, Bronkema, J, Bell, AT., 2004. Application of in situ surface-enhanced Raman spectroscopy (SERS) to the study of citrate oxidation on silica-supported silver nanoparticles. Catal. Lett. 92, 93–99.

Taviot-Gueho, C, Prevot, V, Forano, C, Renaudin, G, Mousty, C, Leroux, F., 2018. Tailoring Hybrid Layered Double Hydroxides for the Development of Innovative Applications. Adv. Funct. Mater. 28, 1703868.

Tran, HN, Lin, CC, Woo, SH, Chao, HP., 2018. Efficient removal of copper and lead by Mg/Al layered double hydroxides intercalated with organic acid anions: Adsorption kinetics, isotherms, and thermodynamics. Appl. Clay Sci. 154, 17–27.

Valeikiene, L, Paitian, R, Grigoraviciute-Puroniene, I, Ishikawa, K, 2019. Kareiva A Transition metal substitution effects in sol-gel derived $Mg_{3-x}M_x/Al_1$ (M = Mn, Co, Ni, Cu, Zn) layered double hydroxides. Mater. Chem. Phys. 237, 121863.

Wang, TL, Liu, MT, Ma, HW, Cao, DF., 2017. Synthesis and characterization of La-doped luminescent multilayer films. J. Chem. 2017, 8203581.

Wang, ZL, Xu, YQ, Tan, L, Zhao, YF, Song, YF., 2020. Recent advance in ultrathin/ultrasmall layered double hydroxides. Chin. Sci. Bull-Chin. 65, 547–564.

Wilhelm, M, Quevedo, MC, Sushkova, A, Galvao, TLP, Bastos, A, Ferreira, M, Tedim, J., 2020. Hexacyanoferrate-intercalated layered double hydroxides as nanoadditives for the detection of early-stage corrosion of steel: The revival of Prussian blue. Eur. J. Inorg. Chem. 2020, 2063–2073.

Xu, ZP, Braterman, PS., 2010. Synthesis, structure and morphology of organic layered double hydroxide (LDH) hybrids: Comparison between aliphatic anions and their oxygenated analogs. Appl. Clay Sci. 48, 235–242.

Xu, S, Zhang, M, Li, SY, Zeng, HY, Tian, XY, Wu, K, Hu, J, Chen, CR, Pan, Y., 2020. Intercalation of a novel containing nitrogen and sulfur anion into hydrotalcite and its highly efficient flame retardant performance for polypropylene. Appl. Clay Sci. 191, 105600.

Zhao, XJ, Zhu, YQ, Xu, SM, Liu, HM, Yin, P, Feng, YL, Yan, H., 2020. Anion exchange behavior of (MAl)-Al-II layered double hydroxides: a molecular dynamics and DFT study. Phys. Chem. Chem. Phys. 22, 19758–19768.

Zheng, Y, Gao, R, Qiu, YS, Zheng, LR, Hu, ZB, Liu, XF., 2021. Tuning Co2+ coordination in cobalt layered double hydroxide nanosheets via Fe3+ doping for efficient oxygen evolution. Inorg. Chem. 60, 5252–5263.

Zohar, I, Forano, C., 2021. Phosphorus recycling potential by synthetic and waste materials enriched with dairy wastewater: a comparative physicochemical study. J. Env. Chem. Eng. 9, 106107.